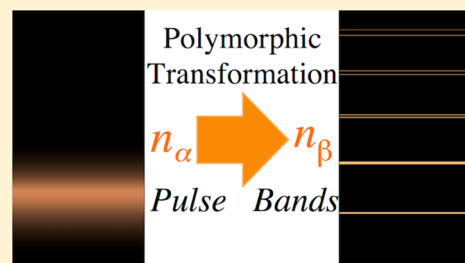


Band Propagation, Scaling Laws, and Phase Transition in a Precipitate System. 2. Computational Study

Andrew Abi Mansour[†] and Mazen Al-Ghoul^{*‡}[†]Department of Chemistry and Center for Theoretical and Computational Nanoscience, Indiana University, Bloomington, Indiana 47405, United States[‡]Department of Chemistry and Program in Computational Science, American University of Beirut, Beirut, Lebanon 11-0236

ABSTRACT: In this second paper, we introduce a chemical kinetic model that investigates the dynamics of the experimental $\text{Ni}^{2+}/\text{NH}_3\text{-OH}^-$ Liesegang system characterized by a pattern of β -nickel hydroxide bands led by a growing pulse of α -nickel hydroxide. The model is based on a system of reaction–diffusion equations describing the precipitation reaction and dissolution of the nickel hydroxide polymorphs by ammonia. The hydroxide ions are assumed to be static whereas ammonia serves as a diffusing “vehicle” that supplies the hydroxide ions along the precipitation zone, and these ions in turn react with the static Ni^{2+} ions. The precipitation–diffusion equations are coupled to nucleation, polymorphic transition, and growth rate equations, each of which is characterized by a critical constant specific to the solid phase dynamics. In the proposed model, priority is given to polymorphic transition rather than nucleation. This implies that the critical constants must be subject to a constraint different than that derived for the Lifshitz–Slyozov instability encountered in classical Liesegang patterns. Numerical simulations confirm the validity of our model and the derived constraint. The pulse position and width are found to scale in time as t^c with $c \approx 0.5$, in agreement with the experimental results. Finally, the mass of the bands is shown to oscillate in time, suggesting competition between growth and polymorphic transition on one side and dissolution on the other.



INTRODUCTION

The Liesegang phenomenon^{1–13} is a special type of self-organized periodic pattern that emerges due to the nonlinear coupling between certain chemical precipitation reactions and diffusion. The resulting patterns might not be static in space and can exhibit rich spatiotemporal dynamics, especially when other transformations, such as redissolution reactions and polymorphic transitions, occur at the same time in the system.^{14–35}

In the first paper of this sequel, we presented an experimental study of a Liesegang system where precipitation of nickel hydroxide and its redissolution in excess ammonia led to fascinating dynamics at the macroscopic as well as at the microscopic levels.⁷ We found that this system, which was prepared by diffusing a concentrated ammonia solution into a gel matrix that contains nickel sulfate, exhibits a propagation of a pulse consisting of solid $\alpha\text{-Ni(OH)}_2$. This was due to the concomitant precipitation reaction between Ni(II) (inner electrolyte) and hydroxide ions (outer electrolyte) and redissolution due to ammonia (also outer electrolyte). As time progresses, the pulse region develops into static multiple Liesegang bands appearing in the region above the Ni(OH)_2 pulse and consisting of the other $\beta\text{-Ni(OH)}_2$ polymorph, as depicted in Figure 1. The distance traveled by the precipitation pulse and its width were shown to exhibit time power laws with exponents close to 0.5. Moreover, we discovered the emergence of a complex mass enrichment mechanism of the formed Liesegang bands displayed by temporal oscillations in the mass

of the $\beta\text{-Ni(OH)}_2$ in the bands whereas the mass of the $\alpha\text{-Ni(OH)}_2$ was found to scale in time as $m \sim t^c$, with c being a function of the initial concentrations of the reactants. In the same paper,⁷ we demonstrated that at the microscopic level, the system undergoes a continuous polymorphic transition with attendant morphological change whereby the solid in the pulse, which consists of nanospheres of α -nickel hydroxide, transforms to form the bands, which consists of larger platelets of α -nickel hydroxide. This clearly indicates the existence of a dynamic Ostwald ripening mechanism^{37,38} that underlies the dynamics at both scales.

The first paper⁷ reports new complexities that have not been reported before in Liesegang systems at the microscopic and macroscopic scales. Although existing theories of Liesegang bands do to a certain degree relate the underlying microscopic physics to the emergent pattern at the macroscopic level, they cannot in their present formulation reproduce the aforementioned newly discovered dynamics at both scales. How, for example, does the observed special Ostwald ripening between the leading front and the trailing bands lead to the scaling behavior of various macroscopic functions and to the mass oscillation in the bands? In this paper, we propose a theoretical paradigm based on a reaction–diffusion mechanism of reactants that is coupled to a nucleation and growth model

Received: May 28, 2015

Revised: August 10, 2015

Published: August 10, 2015

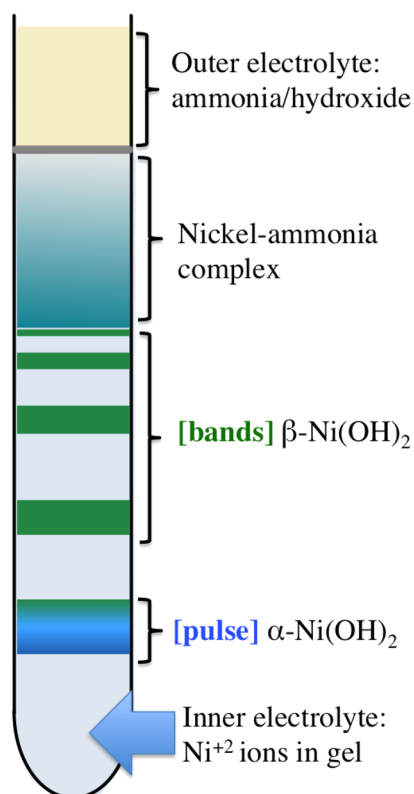


Figure 1. Sketch of a snapshot of the experimental results obtained in the first paper of this sequel.⁷ The pulse moves vertically downward, leaving behind static bands that grow in time and redissolve due to ammonia leaving behind a dissolved nickel complex ion.

based on a simplified dual precipitate model introduced in refs 5, 6, and 14, which takes into account both prenucleation and postnucleation mechanisms that incorporate Ostwald ripening. The essential point lies in the modification of the nucleation mechanism to account for the polymorphic transition and dissolution due to ammonia. On the basis of the experimental results, the polymorphic transition must be subject to a constraint to be determined. The dissolution mechanism must be formulated in such a way that it competes with the growth and polymorphic transformation, which effectively leads to temporal oscillations in the mass of the precipitate.

THEORETICAL METHODS

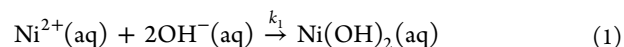
Throughout the paper, we have used the notation $[C]$ to represent the concentration of species C . Because the system under study is heterogeneous and taken for simplicity to be one-dimensional, this function depends on both position x , and time t . At time $t = 0$, the concentration of nickel ions is set to $[Ni^{2+}]_0$ for all $x > 0$, and it is zero for all $x \leq 0$. On the contrary, the initial concentrations of hydroxide ions, ammonia, and ammonium ions are set to $[OH^-]_0$, $[NH_3]_0$, and $[NH_4^+]_0$, respectively, for all $x \leq 0$, and they are zero for all $x > 0$. The initial concentrations of all species are kept constant (Table 1) in all simulations, whereas that of nickel is varied.

Table 1. Initial Concentrations Used in All Simulations for the Ammonia–Ammonium–Hydroxide Reaction

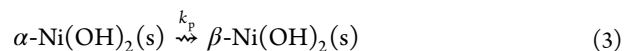
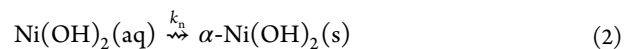
| $[OH^-]_0$ | $[NH_3]_0$ | $[NH_4^+]_0$ |
|------------|-----------------|--------------|
| 3.0 | 5×10^3 | 3.0 |

At time $t > 0$, ammonia starts to diffuse and dissociate whereas the hydroxide ions react with the nickel ions, thus producing a precipitation front that propagates in time. We assume that the final precipitate form and all charged species do not diffuse whereas all neutral species undergo diffusion in the absence of convection.^{39–42} This is based on the experimental fact that the precipitation front propagates from the region rich in hydroxide to the region rich in nickel ions.⁷ The front dynamics must therefore be dictated by diffusion because the equilibrium concentration of nickel is much higher than that of hydroxide. We conclude that ammonia is diffusing much, much faster than the hydroxide and nickel ions, and along the precipitation zone, the ammonia dissociation reaction is far from equilibrium. For simplicity, we have taken the diffusion coefficients of nickel, hydroxide, and ammonium ions to be zero.⁴² This could be due to the electrostatic interaction between these ions and the chemical groups of the gel matrix. All these assumption are validated heuristically by comparing the results of the numerical simulations to the experimental behavior. It is noteworthy that when the same experiment is performed in a different hydrogel matrix (gelatin instead of agar), the exhibited behavior of the system changes radically, which emphasizes the role of the gel and its nature on the emerging pattern.⁴⁷

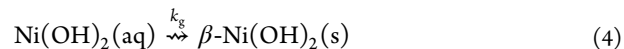
Mechanism. Throughout the analysis, we have assumed that the chemical reactions follow elementary mechanisms such that the rates of the reactions follow the mean-field approximation. Furthermore, we have used the notation \rightarrow to represent a chemical reaction that takes place without any imposed constraints, and \rightsquigarrow to represent a physicochemical change that takes place only when certain conditions are satisfied. The principal chemical reaction taking place in the pores of the gel matrix is



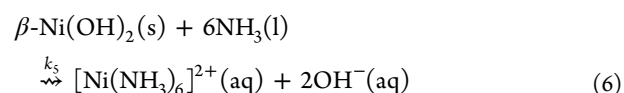
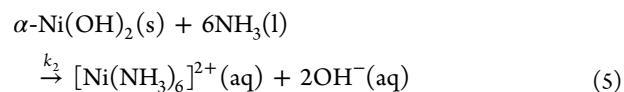
It was shown⁷ that nickel hydroxide crystallizes in the form of α - $Ni(OH)_2(s)$, which then undergoes a polymorphic transition to β - $Ni(OH)_2(s)$. This is mechanistically represented below, for both processes, respectively:



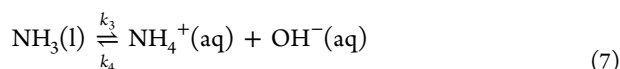
The β - $Ni(OH)_2(s)$ crystals grow from the surrounding $Ni(OH)_2(aq)$ molecules



On the contrary, it was experimentally observed⁷ that ammonia dissolves both the α and β polymorphs via the following complexation reactions



Finally, ammonia undergoes a reversible transformation to form hydroxide and ammonium ions:



Far from the reaction zone, this reaction is effectively at equilibrium. The rates of the outlined processes, and conditions specific to nucleation, growth, polymorphic transition, and dissolution, are discussed in the next subsections.

Rate Functions. Principal Chemical Reaction. Equation 1 describes the chemical reaction between $\text{Ni}^{2+}(\text{aq})$ and $\text{OH}^-(\text{aq})$, and the subsequent formation of the intermediate $\text{Ni}(\text{OH})_2(\text{aq})$. The rate of the chemical reaction is given by

$$v_r = k_1[\text{Ni}^{2+}][\text{OH}^-]^2 \quad (8)$$

where k_1 is the rate constant.

Nucleation, Growth, and Polymorphic Transition. Equation 2 describes the nucleation process, which should be subject to a constraint expressed in terms of a critical nucleation constant c_n , a characteristic parameter of the system. Following the simplified approach introduced in ref 39, the nucleation rate can be written in the form

$$v_n = k_n([\text{Ni}(\text{OH})_2] - c_n)H([\text{Ni}(\text{OH})_2] - c_n) \quad (9)$$

where k_n is a nucleation rate constant and H is the Heaviside unit-step function

$$H([\text{Ni}(\text{OH})_2] - c_n) = \begin{cases} 1 & \forall [\text{Ni}(\text{OH})_2] > c_n \\ 0 & \forall [\text{Ni}(\text{OH})_2] < c_n \\ \frac{1}{2} & \forall [\text{Ni}(\text{OH})_2] = c_n \end{cases} \quad (10)$$

The nucleation rate is taken to be a linear function of $[\text{Ni}(\text{OH})_2]$, and it is positive when $[\text{Ni}(\text{OH})_2] \geq c_n$ whereas for $[\text{Ni}(\text{OH})_2] < c_n$ this rate vanishes. One could model the nucleation process as a nonlinear phenomenon in terms of $[\text{Ni}(\text{OH})_2]$ but this leads to no significant change in the final pattern.^{44–46} Equation 3 describes nucleation and polymorphic transition characterized by a critical constant c_p . The rate of this transition is written in the form

$$v_p = k_p([\text{Ni}(\text{OH})_2] - c_p)H([\text{Ni}(\text{OH})_2] - c_p)[\text{Ni}(\text{OH})_2]_\alpha \quad (11)$$

where k_p is a nucleation and polymorphic rate constant. Equation 4 describes the growth of the β polymorph particles at the expense of the intermediate. The rate of which takes the form

$$v_g = k_g([\text{Ni}(\text{OH})_2] - c_g)H([\text{Ni}(\text{OH})_2] - c_g)[\text{Ni}(\text{OH})_2]_\beta \quad (12)$$

k_g is a growth rate constant, and c_g is the critical value above which growth commences. The choice of the nucleation and growth equations above has been also validated by simulation methods,⁴⁷ which focus on the role of the gel and its concentration in the nucleation process.

Ammonia Dissolution. Equations 5 and 6 account for the dissolution of the α and β polymorphs, respectively, through complexation chemical reactions with ammonia. Equation 7 describes the reversible conversion of ammonia to ammonium and hydroxide ions. The backward rate of ammonia formation is given by

$$v_{c,b} = k_4[\text{OH}^-][\text{NH}_4^+] \quad (13)$$

and the forward rate of ammonia dissociation is given by

$$v_{c,f} = k_3[\text{NH}_3] \quad (14)$$

The rates of dissolution due to ammonia for the α and β polymorphs are, respectively, given by

$$v_{d,\alpha} = k_2[\text{NH}_3]^6[\text{Ni}(\text{OH})_2]_\alpha \quad (15)$$

$$v_{d,\beta} = k_3H([\text{Ni}(\text{OH})_2] - c_d)[\text{NH}_3]^6[\text{Ni}(\text{OH})_2]_\beta \quad (16)$$

The Heaviside function $H([\text{Ni}(\text{OH})_2] - c_d)$ is introduced to prevent ammonia from completely dissolving the β particles. Therefore, for some critical dissolution constant c_d , the dissolution rate $v_{d,\beta}$ must vanish.

Dynamical Equations. Let $\partial_t \rightarrow \partial/\partial t$, then the system of seven coupled partial differential equations describing the complete model is the following:

$$\partial_t[\text{Ni}^{2+}] = -v_r \quad (17)$$

$$\partial_t[\text{OH}^-] = 2(v_{d,\alpha} + v_{d,\beta} - v_r) + v_{c,f} - v_{c,b} \quad (18)$$

$$\partial_t[\text{Ni}(\text{OH})_2] = -\nabla \cdot \mathbf{J}_{\text{Ni}(\text{OH})_2} + v_r - v_n - v_g \quad (19)$$

$$\partial_t[\text{NH}_3] = -\nabla \cdot \mathbf{J}_{\text{NH}_3} - 6(v_{d,\alpha} + v_{d,\beta}) + v_{c,b} - v_{c,f} \quad (20)$$

$$\partial_t[\text{NH}_4^+] = v_{c,f} - v_{c,b} \quad (21)$$

$$\partial_t[\alpha\text{-Ni}(\text{OH})_2] = -\nabla \cdot \mathbf{J}_{\alpha\text{-Ni}(\text{OH})_2} + v_n - v_p - v_{d,\alpha} \quad (22)$$

$$\partial_t[\beta\text{-Ni}(\text{OH})_2] = v_p + v_g - v_{d,\beta} \quad (23)$$

We assume that Fickian diffusion is adequate to describe mass transfer because the dynamics of the Liesegang phenomenon is largely dominated by the asymptotic regime³⁶ (when precipitation begins to dominate over diffusion). Therefore, for species C undergoing diffusion, the flux takes the expression $\mathbf{J}_C = -\Gamma_C \nabla[C]$, where Γ_C is the diffusion coefficient of C .

Polymorphic Transformation and Dissolution Constraints. To obtain the Liesegang pattern, the set of critical constants $\{c_n, c_p, c_g\}$ must be subject to a certain constraint to be determined. Because nucleation in Liesegang systems is a periodic phenomenon, it is necessary that $\max_x c(x,t)$ oscillates around some value, denoted c_m . In the model derived in ref 39, the Lifshitz–Slyozov instability was taken into account by introducing the process of recrystallization or redistribution of matter between particles of the precipitant. That is, the nucleation of $\text{Ni}(\text{OH})_2$ produced smaller particles (called nuclei) that could either grow to form larger particles (the precipitate) or dissolve back to replenish $\text{Ni}(\text{OH})_2$. Therefore, in this case it is necessary that c_m be equal to c_n , and the Lifshitz–Slyozov instability leads to the constraint $c_n > c_p > c_g$. However, in the system we study here, the $\alpha\text{-Ni}(\text{OH})_2$ particles are stable and form a pulse that grows in time, suggesting the continuous formation of the α polymorph and its subsequent conditional transformation to the β hydroxide particles. That is, priority is given here to polymorphic transition (or matter redistribution) rather than nucleation, which means c_m must be equal to c_p . The constraint for the critical constants becomes

$$c_p > c_n > c_g \quad (24)$$

The growth critical constant c_g impacts the frequency of oscillations of $\max_x c(x,t)$ and therefore the magnitude of the distance separating two consecutive bands.

Table 2. Rate Constants for All the Chemical Reactions and Nucleation, Growth, and Dissolution Mechanisms

| \bar{k}_1 | \bar{k}_2 | \bar{k}_3 | \bar{k}_4 | \bar{k}_5 | \bar{k}_n | \bar{k}_g | \bar{k}_p |
|-------------|-------------|-------------|----------------------|---------------------|-------------|-------------|--------------------|
| 10^{-3} | 10^{-26} | 10^{-8} | 5.5×10^{-6} | 2×10^{-24} | 10^{-4} | 10^{-2} | 5×10^{-4} |

The second constraint is derived from the ammonia dissolution of the precipitate. The reason the dissolution phenomenon should be subject to a constraint is the fact that the reaction–diffusion front moves from the region where the concentration of ammonia is high toward the region where the concentration of nickel ions is high. Thus, the precipitate bands can grow for a finite period of time until $c_m < c_g$. At the same time, ammonia invades the region where the precipitate bands are localized, which will eventually lead to their complete dissolution unless the dissolution process is discontinuous in time.

At the time of creation of one band, it is nucleation that dominates followed later by growth of the precipitate. However, if the mass of the precipitate, m_β , is to oscillate in time, dissolution must overcome the nucleation and growth terms in eq 23. This is because ammonia invades the region where the precipitate is localized after growth has commenced. However, as we discussed previously, the dissolution mechanism should cease at a certain point so that the bands do not completely dissolve. Therefore, the mass of the β particles increases when dissolution is negligible (at the onset of the creation of a band) and then decreases when its growth is dominated by dissolution due to ammonia. This in theory leads to oscillations of m_β in time. As the nucleation wave (represented by the α particles) moves away from the precipitation region, $[\text{Ni}(\text{OH})_2]$ eventually drops below c_d , and dissolution ceases. This prevents the bands from completely dissolving, as observed in the experiments.⁷

RESULTS AND DISCUSSION

The Liesegang experiment in the first paper⁷ was carried out in a long cylindrical thin tube (of length L and diameter ~ 7 mm)

Table 3. Values of Diffusion Coefficients and Critical Constants Used in All Simulations

| $\bar{\Gamma}_{\text{Ni}(\text{OH})_2}$ | $\bar{\Gamma}_{\text{NH}_3}$ | $\bar{\Gamma}_{\alpha\text{-Ni}(\text{OH})_2}$ | \bar{c}_d | \bar{c}_g | \bar{c}_n | \bar{c}_p |
|---|------------------------------|--|-------------|-------------|-------------|-------------|
| 0.1 | 0.5 | 0.2 | 0.65 | 0.7 | 0.8 | 1.0 |

with a vertical x -direction. Because of the large aspect ratio and the symmetry of reactor, the system can be assumed to be quasi-1D along the x -direction. Let $\partial_x \rightarrow \partial/\partial_x$, then the dimensionless form of eqs 17–23 becomes

$$\partial_t[\text{Ni}^{2+}] = -\bar{v}_r \quad (25)$$

$$\partial_t[\text{OH}^-] = 2(\bar{v}_{d,\alpha} + \bar{v}_{d,\beta} - \bar{v}_r) + \bar{v}_{c,f} - \bar{v}_{c,b} \quad (26)$$

$$\partial_t[\text{Ni}(\text{OH})_2] = -\partial_x J_{\text{Ni}(\text{OH})_2} + \bar{v}_r - \bar{v}_n - \bar{v}_g \quad (27)$$

$$\partial_t[\text{NH}_3] = -\partial_x J_{\text{NH}_3} - 6(\bar{v}_{d,\alpha} + \bar{v}_{d,\beta}) + \bar{v}_{c,b} - \bar{v}_{c,f} \quad (28)$$

$$\partial_t[\text{NH}_4^+] = \bar{v}_{c,f} - \bar{v}_{c,b} \quad (29)$$

$$\partial_t[\alpha\text{-Ni}(\text{OH})_2] = -\partial_x J_{\alpha\text{-Ni}(\text{OH})_2} + \bar{v}_n - \bar{v}_p - \bar{v}_{d,\alpha} \quad (30)$$

$$\partial_t[\beta\text{-Ni}(\text{OH})_2] = \bar{v}_p + \bar{v}_g - \bar{v}_{d,\beta} \quad (31)$$

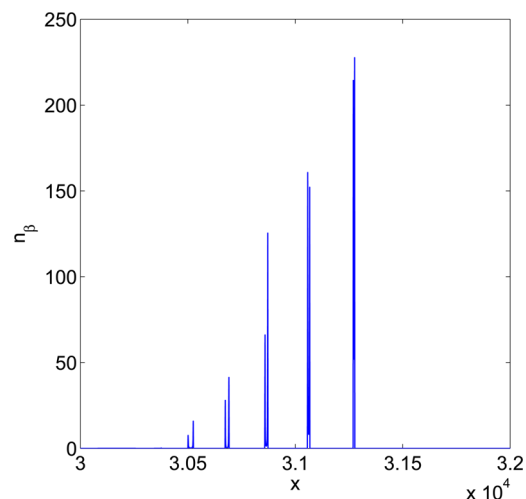


Figure 2. Spatial distribution of n_β (at $t = 10^6$) follows the Liesegang pattern in which the precipitate takes the form of a discrete set of bands characterized by an increasing distance of separation. The initial concentration of nickel ions was taken to be 100.0.

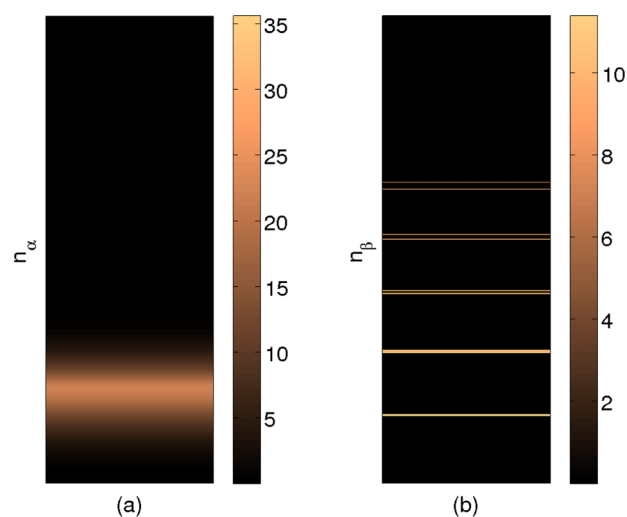


Figure 3. Colormap plot at $t = 10^6$ for the α -nickel hydroxide front (a) forming a pulse that moves downward, leaving behind static bands (b) that grow in time. The initial concentration of nickel ions was taken to be 100.0.

where t represents dimensionless time, which is real time scaled by $[\text{NH}_3]_0^3 L^{-1} \sqrt{k_5 \bar{\Gamma}_{\text{NH}_3}}$, the spatial derivative is with respect to the dimensionless variable x , which is real space scaled by L^{-1} , all concentration functions are dimensionless (scaled by c_p^{-1}), and

$$\bar{v}_r = \bar{k}_1[\text{Ni}^{2+}][\text{OH}^-]^2 \quad (32)$$

$$\bar{v}_{d,\alpha} = \bar{k}_2[\text{NH}_3]^6[\text{Ni}(\text{OH})_2]_\alpha \quad (33)$$

$$\bar{v}_{c,f} = \bar{k}_3[\text{NH}_3] \quad (34)$$

$$\bar{v}_{c,b} = \bar{k}_4[\text{OH}^-][\text{NH}_4^+] \quad (35)$$

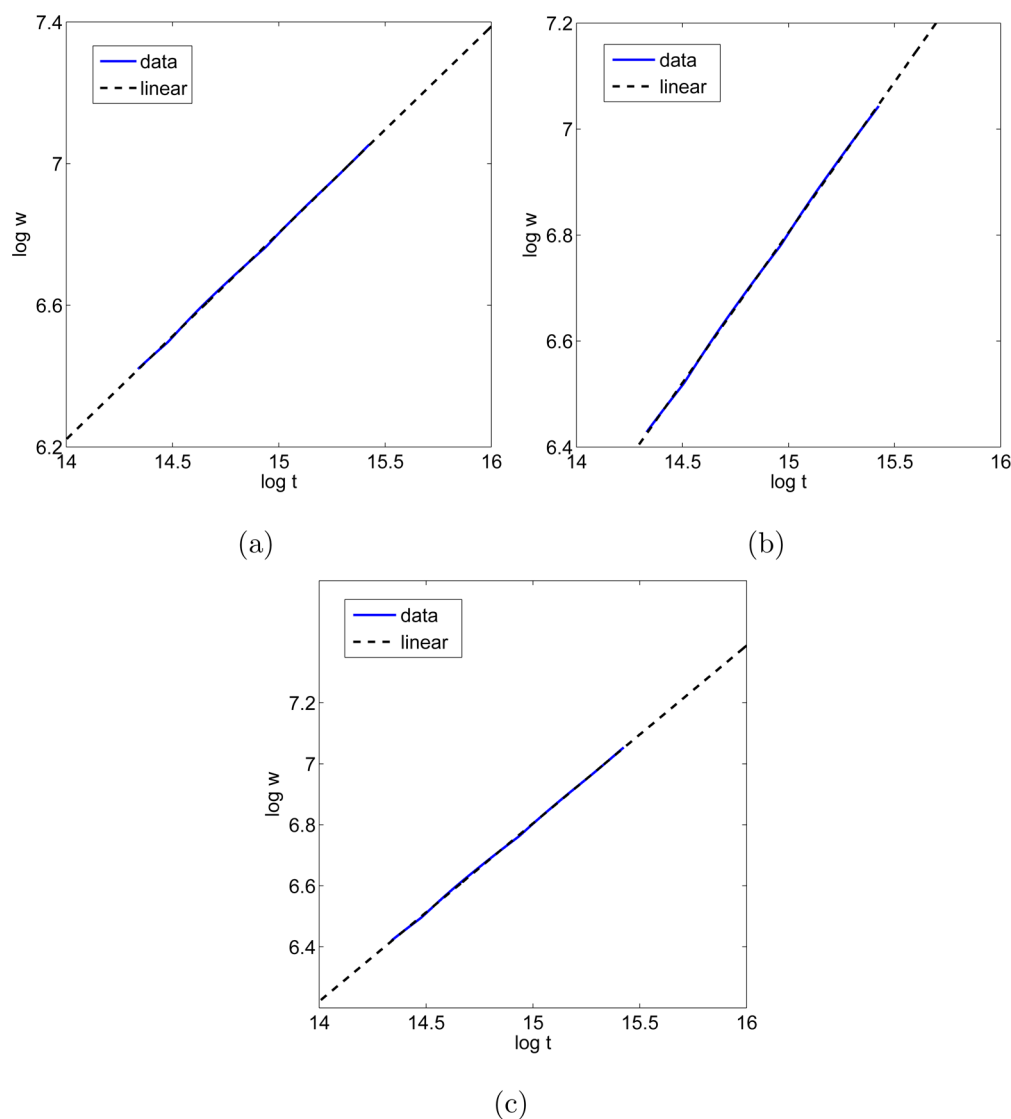


Figure 4. Logarithmic plots of the width of the α -nickel hydroxide front as a function of time, t , for various inner concentrations of nickel: (a) 50.0; (b) 100.0; (c) 150.0. By linear regression, the slopes are found to be equal to (a) 0.5831, (b) 0.5678, and (c) 0.5629.

$$\bar{v}_{\alpha,\beta} = \bar{k}_3 H([\text{Ni}(\text{OH})_2] - \bar{c}_d) [\text{NH}_3]^6 [\text{Ni}(\text{OH})_2]_\beta \quad (36)$$

$$\bar{v}_n = \bar{k}_n ([\text{Ni}(\text{OH})_2] - \bar{c}_n) H([\text{Ni}(\text{OH})_2] - \bar{c}_n) \quad (37)$$

$$\bar{v}_p = \bar{k}_p ([\text{Ni}(\text{OH})_2] - \bar{c}_p) H([\text{Ni}(\text{OH})_2] - \bar{c}_p) [\text{Ni}(\text{OH})_2]_\alpha \quad (38)$$

$$\bar{v}_g = \bar{k}_g ([\text{Ni}(\text{OH})_2] - \bar{c}_g) H([\text{Ni}(\text{OH})_2] - \bar{c}_g) [\text{Ni}(\text{OH})_2]_\beta \quad (39)$$

where

$$\bar{k}_1 = \frac{k_1 L c_p^2}{[\text{NH}_3]_0^3 \sqrt{k_5 \Gamma_{\text{NH}_3}}} \quad (40)$$

$$\bar{k}_2 = \frac{k_2 L c_p^6}{[\text{NH}_3]_0^3 \sqrt{k_5 \Gamma_{\text{NH}_3}}} \quad (41)$$

$$\bar{k}_3 = \frac{k_3 L}{[\text{NH}_3]_0^3 \sqrt{k_5 \Gamma_{\text{NH}_3}}} \quad (42)$$

$$\bar{k}_4 = \frac{k_4 L c_p}{[\text{NH}_3]_0^3 \sqrt{k_5 \Gamma_{\text{NH}_3}}} \quad (43)$$

$$\bar{k}_5 = \frac{L c_p^6}{[\text{NH}_3]_0^3} \sqrt{\frac{k_5}{\Gamma_{\text{NH}_3}}} \quad (44)$$

$$\bar{k}_n = \frac{k_n L}{[\text{NH}_3]_0^3 \sqrt{k_5 \Gamma_{\text{NH}_3}}} \quad (45)$$

$$\bar{k}_p = \frac{k_p L c_p}{[\text{NH}_3]_0^3 \sqrt{k_5 \Gamma_{\text{NH}_3}}} \quad (46)$$

$$\bar{k}_g = \frac{k_g L c_p}{[\text{NH}_3]_0^3 \sqrt{k_5 \Gamma_{\text{NH}_3}}} \quad (47)$$

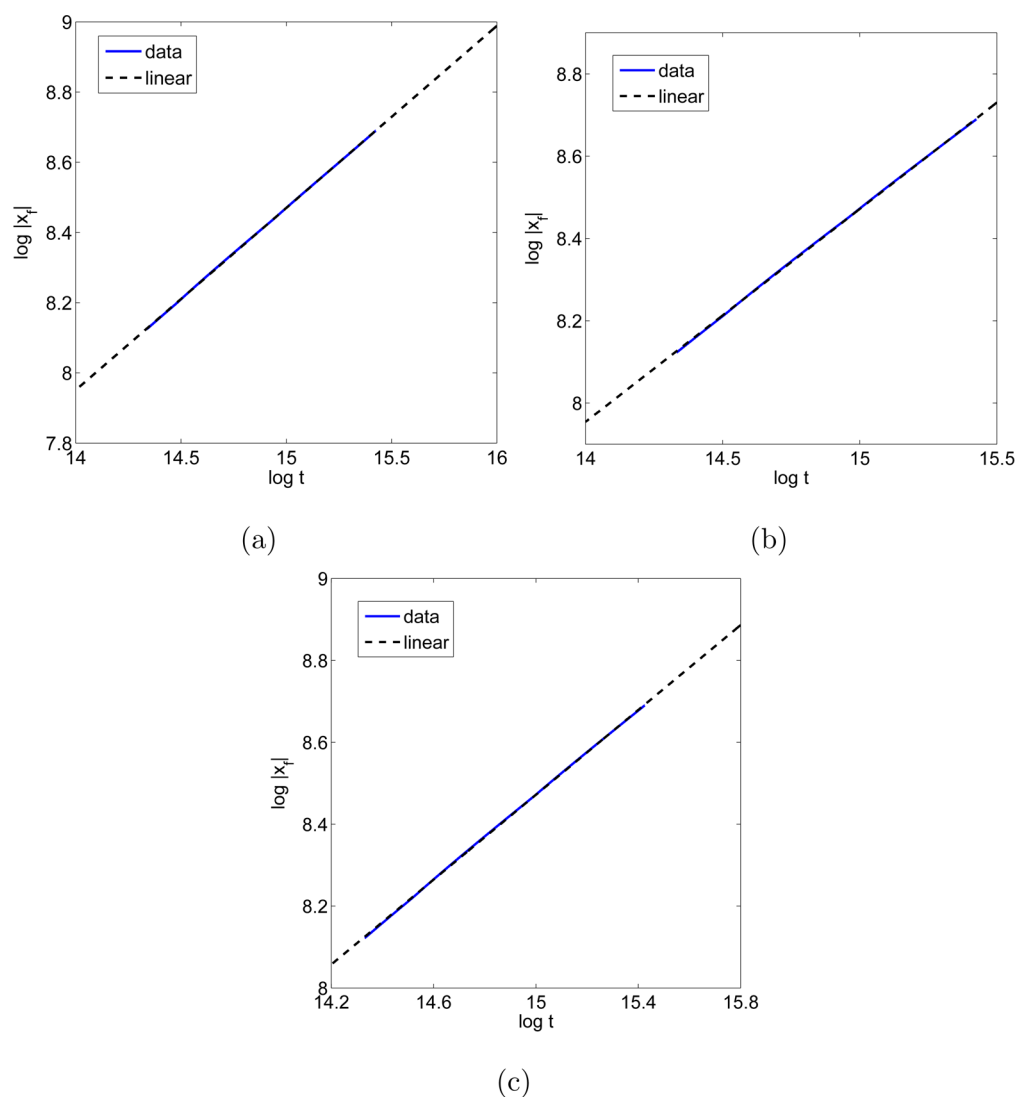


Figure 5. Logarithmic plots of the absolute value of the front position ($|x_f|$) for the α -nickel hydroxide as a function of time, t , for various initial inner concentrations of nickel: (a) 50.0; (b) 100.0; (c) 150.0. By linear regression, the slopes are found to be equal to (a) 0.5187, (b) 0.5174, and (c) 0.5181.

and $\bar{c}_n = c_n/c_p$, $\bar{c}_p = 1$, $\bar{c}_g = c_g/c_p$, and $\bar{\Gamma}_C = \Gamma_C/L[\text{NH}_3]_0^3\sqrt{k_5\Gamma_{\text{NH}_3}}$ for species C.

The central finite difference method⁴³ is used to numerically solve eqs 25–31 with the constraint imposed on the critical constants eq 24. Numerical simulations are done in one dimension over a set of 60 000 points, with a resolution of 0.5. The values for the various kinetic parameters used in the simulations are shown in Tables 2 and 3.

At initial time, a band of α -nickel hydroxide (n_α) starts forming near the interface and as it starts propagating downward, its width starts increasing. As soon as the band moves away from the interface, a static band of the other polymorph β -nickel hydroxide (n_β) appears. After a relatively long time, a Liesegang pattern consisting of multiple bands of β -nickel hydroxide has formed in the wake of thick band of α -nickel hydroxide as shown in Figures 2 and 3, which agrees with the experimental results.⁷

The spatiotemporal dynamics of the leading propagating band of the α -nickel hydroxide particles are then explored. The position, x_f , of the α band is numerically computed for various initial concentrations of the inner electrolyte (nickel) as shown

in Figure 5. It exhibits the scaling law $x_f \sim t^a$, where $a \approx 0.5$ and independent of the concentration of nickel ions, which agrees with the experimental results and confirms the diffusion-limited nature of the dynamics. The width of the pulse of α is also computed for various concentrations of nickel ions as shown in Figure 4. Its temporal dynamics also exhibits a scaling law of the form $w \sim t^b$, where $b \approx 0.5$ and independent of the concentration of nickel ions, which also agrees with the experimental findings.⁷ In the presence of strong dissolution, however, this scaling is lost. Furthermore, significant temporal oscillations in the pulse width and position are observed when dissolution dominates over growth. Such oscillations were negligible in the experimental study. Therefore, we conclude that the reaction of ammonia with the α pulse was not significant. Time variation in mass of the particles in the pulse and bands region, m_α and m_β , was also computed and compared to experiment. The results for the pulse are shown in Figure 6, where a power law of the form $m_\alpha \sim t^c$ is obtained. On the contrary, the total mass of the bands, m_β , is shown to oscillate in time (Figure 7), thus reproducing the complex experimental behavior: static bands do not indicate a static mass but on the

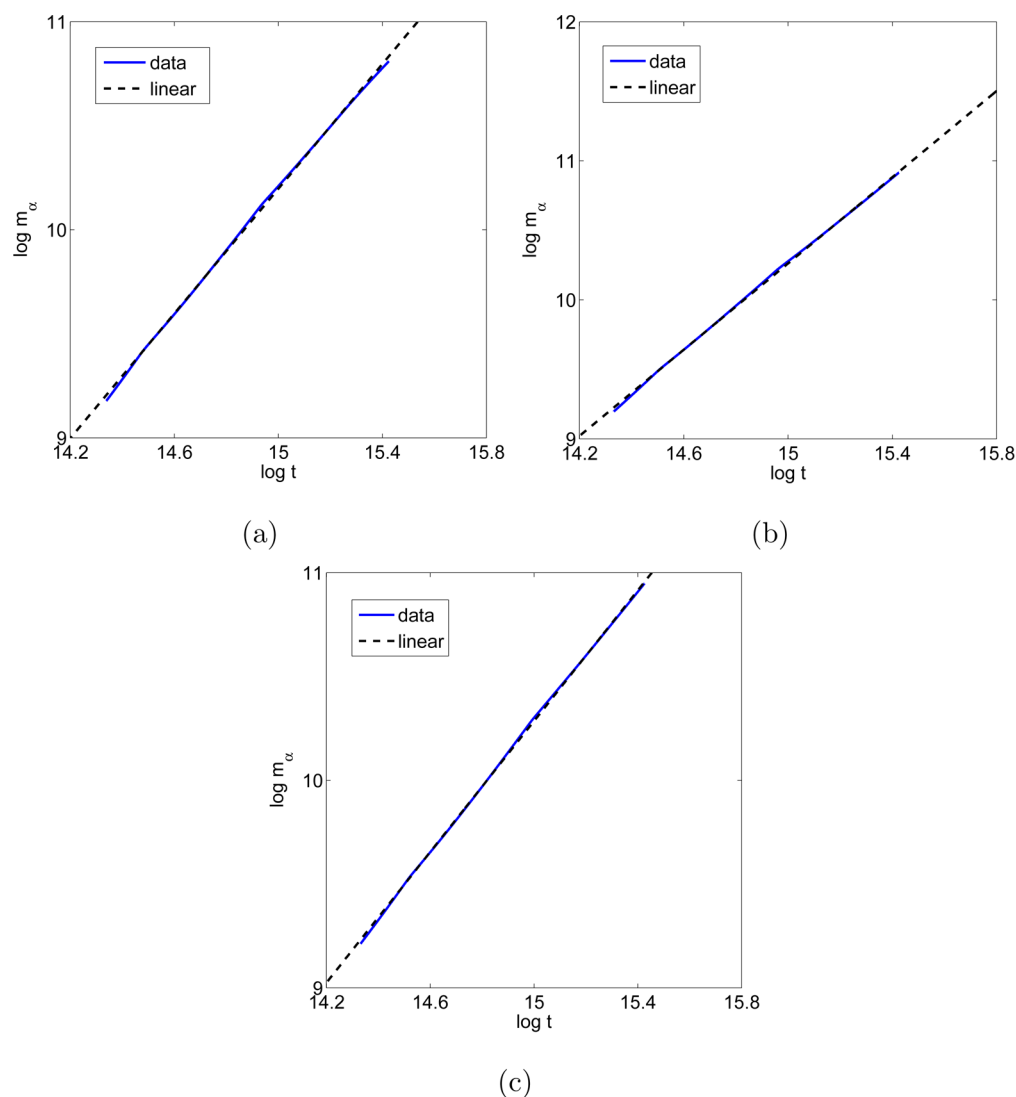


Figure 6. Logarithmic plots of the mass of the α -nickel hydroxide front for various concentrations of nickel ions: 50.0 (blue); 100.0 (teal); 150.0 (black). By linear regression, the slopes are found to be 1.50, 1.55, and 1.57, respectively.

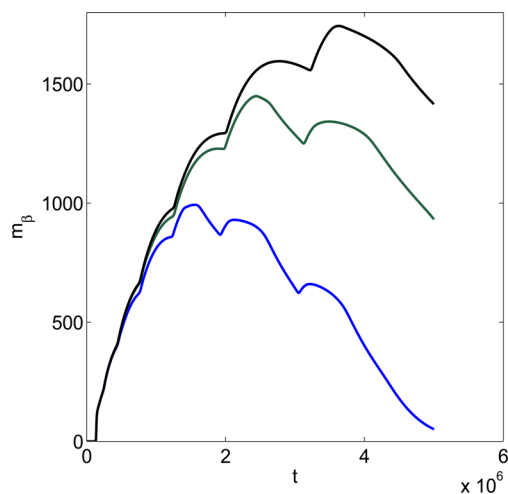


Figure 7. Temporal oscillations in the mass of the precipitate in the bands region for various initial concentrations of nickel ions: 50.0 (blue); 100.0 (teal); 150.0 (black). The oscillations in the mass imply competition between nucleation and growth on one hand and dissolution due to ammonia on the other.

contrary there is a continuous redissolution–reprecipitation mass enriching mechanism that dominates the bands region.

CONCLUSIONS

We introduced a chemical kinetic model based on a reaction–diffusion mechanism coupled to nucleation and growth. The model reproduced the scaling laws and captured the mass dynamics of the experimental Liesegang system reported previously.⁷ This system was characterized by a pattern of β -nickel hydroxide bands led by a growing pulse of α -nickel hydroxide. In the evolution equations, polymorphic transition took precedence over nucleation, which led to a constraint on the critical constants different than the one imposed by the Lifshitz–Slyozov instability encountered in classical Liesegang patterns. In the third sequel, which will be submitted shortly, we will show the importance of the pulse region in dictating the type of bands that emerge from it. In that regard, the anions in the gel will be shown to play a decisive role due to its interaction with the α polymorph in the pulse.

AUTHOR INFORMATION

Corresponding Author

*M. Al-Ghoul. Phone: +961 (1)350 000. Fax: +961 (1)365 217. E-mail: mazen.ghoul@aub.edu.lb.

Notes

The authors declare no competing financial interest.

ACKNOWLEDGMENTS

This work is supported by the Lebanese National Council for Scientific Research and by the American University of Beirut Research Board.

REFERENCES

- (1) Liesegang, R. E. *Chemische Fernwirkung. Lieseg. Photograph. Arch.* **1896**, *37*, 305.
- (2) Dayeh, M.; Ammar, M.; Al-Ghoul, M. Transition from Rings to Spots in a Precipitation Reaction-Diffusion System. *RSC Adv.* **2014**, *4*, 60034–60038.
- (3) Grzybowski, B. *Chemistry in Motion: Reaction-Diffusion Systems for Micro- and Nanotechnology*; John Wiley & Sons: Chichester, U.K., 2009.
- (4) Hensch, H. *Crystals in Gels and Liesegang Rings*; Cambridge University Press: Cambridge, U.K., 1988.
- (5) Al-Ghoul, M.; Sultan, R. Front Propagation in Patterned Precipitation. 1. Simulation of a Migrating $\text{Co}(\text{OH})_2$ Liesegang Pattern. *J. Phys. Chem. A* **2001**, *105*, 8053–8058.
- (6) Al-Ghoul, M.; Sultan, R. Front Propagation in Patterned Precipitation. 2. Electric Effects in Precipitation-Dissolution Patterning Schemes. *J. Phys. Chem. A* **2003**, *107*, 1095–1101.
- (7) Al-Ghoul, M.; Ammar, M.; Al-Kayssi, R. Band Propagation, Scaling Laws and Phase Transition in a Precipitate System. I: Experimental Study. *J. Phys. Chem. A* **2012**, *116*, 4427–4437.
- (8) Shreif, Z.; Mandalian, L.; Abi-Haydar, A.; Sultan, R. Taming Ring Morphology in 2D $\text{Co}(\text{OH})_2$ Liesegang Patterns. *Phys. Chem. Chem. Phys.* **2004**, *6*, 3461–3466.
- (9) Batlouni, H.; El-Rassy, H.; Al-Ghoul, M. Cosynthesis, Coexistence, and Self-Organization of α - and β -Cobalt Hydroxide Based on Diffusion and Reaction in Organic Gels. *J. Phys. Chem. A* **2008**, *112*, 7755–7757.
- (10) Al-Ghoul, M.; El-Rassy, H.; Coradin, T.; Mokalled, T. Reaction-Diffusion Based Co-Synthesis of Stable α - and β -Cobalt Hydroxide in Bio-Organic Gels. *J. Cryst. Growth* **2010**, *312*, 856–862.
- (11) Al-Ghoul, M.; Ghaddar, T.; Moukalled, T. Pulse-front Propagation and Interaction During the Growth of CdS Nanoparticles in a Gel. *J. Phys. Chem. B* **2009**, *113*, 11594–11603.
- (12) Nasreddine, V.; Sultan, R. Propagating Fronts and Chaotic Dynamics in $\text{Co}(\text{OH})_2$ Liesegang Systems. *J. Phys. Chem. A* **1999**, *103*, 2934–2940.
- (13) Lloyd, F. E.; Moravec, V. Studies in Periodic Precipitation. *Plant Physiol.* **1928**, *3*, 101–130.
- (14) Al-Ghoul, M.; Experimental and Theoretical Study of the Dynamics of a Propagating Liesegang System. In *Precipitation Patterns in Reaction-Diffusion Systems*; Lagzi, I., Ed.; Research Signpost: Kerala, India, 2010; pp 117–139.
- (15) Das, I.; Pushkarna, A.; Argawal, N. R. Chemical Waves and Light-Induced Spatial Bifurcation in the Mercuric Chloride-Potassium Iodide System in Gel Media. *J. Phys. Chem.* **1989**, *93*, 7269–7275.
- (16) Das, I.; Pushkarna, A.; Bhattacharjee, A. New Results on Light-Induced Spatial Bifurcation and Electrical Field Effect on Chemical Waves in the Mercury (II) Chloride-Potassium Iodide System in Gel Media. *J. Phys. Chem.* **1990**, *94*, 8968–8973.
- (17) Ayass, M.; Lagzi, I.; Al-Ghoul, M. Three-Dimensional Superdiffusive Chemical Waves in a Precipitation System. *Phys. Chem. Chem. Phys.* **2014**, *16*, 24656–24660.
- (18) Ayass, M.; Abi Mansour, A.; Al-Ghoul, M. Alternating Metastable/Stable Pattern in the Mercuric Iodide Crystal Formation Outside the Ostwald Rule of Stages. *J. Phys. Chem. A* **2014**, *118*, 7725–7731.
- (19) Ayass, M.; Al-Ghoul, M. Superdiffusive Cusp-Like Waves in the Mercuric Iodide Precipitate System and Their Transition to Regular Reaction Bands. *J. Phys. Chem. A* **2014**, *118*, 3857–3865.
- (20) Zrinyi, M.; Galfi, L.; Smidroczi, E.; Racz, Z.; Horkay, F. Direct Observation of a Crossover from Heterogeneous Traveling Wave to Liesegang Pattern Formation. *J. Phys. Chem.* **1991**, *95*, 1618–1620.
- (21) Ayass, M.; Al-Ghoul, M.; Lagzi, I. Chemical Waves in Heterogeneous Media. *J. Phys. Chem. A* **2014**, *118*, 11678–16782.
- (22) Lagzi, I. Simulation of Liesegang Patterns: Effect of Reversible Complex Formation of Precipitate. *J. Phys. Chem. B* **2003**, *107*, 13750–13753.
- (23) Izsak, F.; Lagzi, I. Simulation of a Crossover from the Precipitation Wave to Moving Liesegang Pattern Formation. *J. Phys. Chem. A* **2005**, *109*, 730–733.
- (24) Lagzi, I.; Ueyama, D. Pattern Transition Between Periodic Liesegang Pattern and Crystal Growth Regime in Reaction-Diffusion Systems. *Chem. Phys. Lett.* **2009**, *468*, 188–192.
- (25) Lide, D. *CRC Handbook of Chemistry and Physics*, 87th ed.; CRC Press: Boca Raton, FL, 2004–2005.
- (26) Rajamathi, M.; Subbanna, G.; Kamath, P. V. On the Existence of a Nickel Hydroxide Phase which is neither α nor β . *J. Mater. Chem.* **1997**, *7*, 2293–2296.
- (27) Rajamathi, M.; Kamath, P. V.; Seshadri, R. Polymorphism in Nickel Hydroxide: Role of Interstratification. *J. Mater. Chem.* **2000**, *10*, 503–506.
- (28) Rajamathi, M.; Kamath, P. V. Anionic Clay-Like Behaviour of α -nickel Hydroxide: Chromate Sorption Studies. *Mater. Lett.* **2003**, *57*, 2390–2394.
- (29) Yamaguchi, N. U.; Scheinost, A. C.; Sparks, D. L. Surface-Induced Nickel Hydroxide Precipitation in the Presence of Citrate and Salicylate. *Soil Sci. Soc. Am. J.* **2001**, *65*, 729–736.
- (30) Hahn, F.; Beden, B.; Croissant, M. J.; Lamy, C. In Situ UV Visible Reflectance Spectroscopic Investigation of the Nickel Electrode-Alkaline Solution Interface. *Electrochim. Acta* **1986**, *31*, 335–342.
- (31) Miessler, G.; Tarr, D. A. *Inorganic Chemistry*, 4th ed.; Pearson: USA, 2011.
- (32) Fu, G.; Hu, Z.; Xie, L.; Jin, X.; Xie, Y.; Wang, Y.; Zhang, Z.; Yang, Y.; Wu, H. Electrodeposition of Nickel Hydroxide Films on Nickel Foil and Its Electrochemical Performances for Supercapacitor. *Int. J. Electrochem. Sci.* **2009**, *4*, 1052–1062.
- (33) Dong, L.; Chu, Y.; Sun, W. Controllable Synthesis of Nickel Hydroxide and Porous Nickel Oxide Nanostructures with Different Morphologies. *Chem. - Eur. J.* **2008**, *14*, 5064–5072.
- (34) Liang, Z.; Zhu, Y.; Hu, X. α -nickel Hydroxide Nanosheets and Their Thermal Decomposition to Nickel Oxide Nanosheets. *J. Phys. Chem. B* **2004**, *108*, 3488–3491.
- (35) Du, Y.; Ok, M.; O'Hare, D. A Kinetic Study of the Phase Conversion of Layered Cobalt Hydroxides. *J. Mater. Chem.* **2008**, *18*, 4450–4459.
- (36) Abi Mansour, A.; Al-Ghoul, M. Scaling and Crossover Dynamics in the Hyperbolic Reaction-Diffusion Equations of Initially Separated Components. *Phys. Rev. E* **2011**, *84*, 26107–26119.
- (37) Ostwald, S. Studies on Formation and Transformation of Solid Materials. *Z. Phys. Chem.* **1897**, *22*, 289–330.
- (38) Greenwell, H. C.; Bindley, L. A.; Unwin, P. R.; Holliman, P. G.; Jones, W.; Coveney, P. V.; Barnes, S. L. In Situ Monitoring of Crystal Growth and Dissolution of Oriented Layered Double-Hydroxide Crystals Immobilized on Silicon. *J. Cryst. Growth* **2006**, *294*, 53–59.
- (39) Chernavskii, D. S.; Polezhaev, A. A.; Muller, S. C. A Model of Pattern Formation by Precipitation. *Phys. D* **1991**, *54*, 160–170.
- (40) Polezhaev, A. A.; Muller, S. C.; Polezhaev, A. A. Complexity of Precipitation Patterns: Comparison of Simulation with Experiment. *Chaos* **1994**, *4*, 631–636.
- (41) Molnar, F.; Izsak, F.; Lagzi, I. Design of Equidistant and Revert Type Precipitation Patterns in Reaction-Diffusion Systems. *Phys. Chem. Chem. Phys.* **2008**, *10*, 2368–2373.

- (42) Gu, W. Y.; Yao, H.; Vega, A. L.; Flager, D. Diffusivity of Ions in Agarose Gels and Intervertebral Disc: Effect of Porosity. *Ann. Biomed. Eng.* **2004**, *32*, 1710–1717.
- (43) Thomas, J. W. *Numerical Partial Differential Equations: Finite Difference Methods*; Springer: New York, 1998.
- (44) Nocedal, J.; Wright, J. S. *Numerical Optimization*; Springer: New York, 2000.
- (45) Abi Mansour, A.; Al-Ghoul, M. Vertex-Based Finite Volume Simulation of Liesegang Patterns on Structureless Meshes. *Phys. Rev. E* **2014**, *89*, 033303–033310.
- (46) Al-Ghoul, M.; Sultan, R. Front Propagation in Patterned Precipitation. 1. Simulation of a Migrating $\text{Co}(\text{OH})_2$ Liesegang Pattern. *J. Phys. Chem. A* **2001**, *105*, 8053–8058.
- (47) Chen, L.; Kang, Q.; He, Y.; Tao, W. Mesoscopic Study of the Effects of Gel Concentration and Materials on the Formation of Precipitation Patterns. *Langmuir* **2012**, *28*, 11745–11754.